Heterogeneity Analysis on Multi-state Brain Functional Connectivity and Adolescent Neurocognition

Shiying Wang¹, Todd Constable², Heping Zhang^{1*}, and Yize Zhao^{1*}

¹Department of Biostatistics, Yale University, New Haven, CT

²Department of Radiology & Biomedical Imaging,

Yale University, New Haven, CT

Abstract

Brain functional connectivity or connectome, a unique measure for brain functional organization, provides a great potential to explain the neurobiological underpinning of behavioral profiles. Existing connectome-based analyses highly concentrate on brain activities under a single cognitive state, and fail to consider heterogeneity when attempting to characterize brain-to-behavior relationships. In this work, we study the complex impact of multi-state functional connectivity on behaviors by analyzing the data from a recent landmark brain development and child health study. We propose a nonparametric, Bayesian supervised heterogeneity analysis to uncover neurodevelopmental subtypes with distinct effect mechanisms. We impose stochastic block structures to identify network-based functional phenotypes and develop a variational expectation—maximization algorithm to facilitate an efficient posterior computation. Through integrating resting-state and task-related functional connectomes, we dissect heterogeneous effect mechanisms on children's fluid intelligence from the functional network phenotypes including Fronto-parietal Network and Default Mode Network under different cognitive states. Meanwhile, our method improves the prediction of children's fluid intelligence compared with existing alternatives and single state analyses. Based on extensive simulations, we further confirm the superior performance of our method on uncovering brain-to-behavior relationships.

Keywords: Bayesian modeling; Functional connectivity; Heterogeneity analysis; Stochastic block model; Variational algorithm

Correspondence should be directed to: vize.zhao@yale.edu and heping.zhang@yale.edu

1 Introduction

Functional magnetic resonance imaging (fMRI), a non-invasive neuroimaging technique, has rapidly developed over the past decades and evolved into a powerful tool to study brain functions during cognitive states (Blakemore, 2012; Morita et al., 2016). FMRI-based functional connectivity (functional connectome), defined as the dependency of neuronal activity patterns among spatially-distinct brain regions (Friston et al., 1993), reflects the brain functional synchronization, and provides a great potential to reveal how the brain develops, learns, and ages, and how it is affected by diseases.

Though the canonical functional connectome is defined under resting-state, recent studies show that task-based fMRI also provides crucial information to understand cognitive behaviors (Greene et al., 2018; Gonzalez-Castillo and Bandettini, 2018). Specifically, under resting-state, brain functional connectivity exhibits intrinsic network structures, where regions with strong connections form sub-networks (Fox and Raichle, 2007). Under tasks, functional connectivity reflects brain synchronous responses to tasks and has been shown to amplify trait-relevant individual differences (Greene et al., 2018). To a certain extent, resting-and task-state connectivity provide complementary information on the brain functional organizations. Thus, it is potentially useful to integrate multi-state functional connectivity to study the neurobiological underpinning of behavioral profiles. We investigate this point by analyzing the data from the Adolescent Brain Cognitive Development study (ABCD) study.

Launched in 2015, the ABCD study is the largest prospective study to investigate brain development and adolescent health by following more than 10,000 children aged 9 to 10 years from 21 sites across the United States (Garavan et al., 2018). The study collects a wealth of measures of youths, including neuroimaging, cognitive, behavioral, and youth and parent self-report metrics (Karcher and Barch, 2021). It provides a unique opportunity to investigate how the functional organizations of brain impact cognitive behaviors in adolescence, a critical

and sensitive period of brain development.

We focus on the baseline ABCD data (Released 3.0.1) and fMRI data available through Fast Track option as of April 2018 with data released for 5,772 participants. Detailed imaging acquisition and processing across different sites are described in Hagler Jr et al. (2019) and Casey et al. (2018). Briefly, for the neuroimaging processes, each participant went through a scan session on a fixed order beginning with a localizer, acquisition of 3D T1-weighted images, 2 runs of resting-state fMRI, diffusion weighted images, T2-weighted images, 1-2 runs of resting-state fMRI and task-based fMRI. The task-based fMRI consists of three tasks: an emotional version of the n-back task (EN-back), the Monetary Incentive Delay (MID) task, and the Stop Signal task (SST). These tasks measure six domains of function: working memory, emotion regulation, reward processing, motivation, impulsivity, and impulse control. Our goal here is to investigate how brain functional organizations, particularly the ones reflected through connectivity under different cognitive states, impact children's behaviors (e.g., fluid intelligence, mental ability).

There has been a great interest to build connectome-based predictive models by linking functional connectivity with behavioral traits. The unique network structure of connectomes led to the development of various analytical solutions. One approach is to summarize connectome measures by scalar metrics (Van Den Heuvel et al., 2009; Cohen and D'Esposito, 2016; Vriend et al., 2020) or unique edges (Shen et al., 2017; Gao et al., 2019), and model their impact on an outcome trait under regression models. However, existing methods tend to ignore the topographic relationships among brain regions and destroy the network structure. As an alternative, tensor regressions (Zhou et al., 2013; Li et al., 2018) have been proposed and extended to brain connectome application (Xu, 2020) under a symmetric constraint. Regardless of their potential for preserving the network topology, the biological interpretation of tensor-based methods is arguably not straightforward.

Beyond the challenges of analyzing the connectome data noted above, the heterogeneity

in the connectivity-to-behavior relationships across a population is generally understudied. Particularly, we expect such heterogeneity analysis is supervised to reflect the complex effect mechanism from brain functional organizations to behavioral traits. Supervised heterogeneity analysis has already been incorporated in cancer studies and other complex traits (Im et al., 2021; Shen and He, 2015) to investigate subtypes with different responses to treatment patterns, but has rarely been considered in cognitive studies and neuroscience. In our application, we focus on children in their adolescence. Existing literature has revealed that both the brain organization and cognitive abilities remain in an active alternating state during adolescence (Arain et al., 2013). Therefore, we expect different children may employ distinct brain-to-behavior effect paradigms, leading to different neurodevelopmental subtypes. Assessing the heterogeneity will provide useful information in understanding human cognition and developing future personalized interventions. From an analytical perspective, both frequentist and Bayesian approaches have been proposed for supervised heterogeneity analyses, including tree-based methods (Zhang and Singer, 2010) and mixture models (Shen and He, 2015; Berger et al., 2014; Fruhwirth-Schnatter et al., 2019). However, these existing methods are not applicable to our problem involving multi-state connectome predictors.

In this study, we develop a Bayesian supervised heterogeneity analysis to associate multistate brain functional connectivity with a behavior outcome. Specifically, we develop a hierarchical model to jointly dissect the modular configuration of each state-specific functional connectivity via stochastic block structures, and model the outcome trait under latent sub-network level connectivity strength from different cognitive states. To characterize heterogeneity, we assume subjects belongs to an unknown number of subtypes, and propose a nonparametric supervised clustering to uncover different effect mechanisms within the population. To further identify functional network phenotypes to define each subtype, we impose shrinkage to select informative cluster-specific and state-specific sub-network features. We finally develop a variational expectation—maximization (VEM) algorithm to achieve posterior computation under an efficient computation.

The remainder of this article is organized as follows. We describe our Bayesian model and posterior algorithm in Section 2. We present the ABCD data analysis on multi-state brain functional connectivity in Section 3, followed by extensive simulation studies in Section 4. We finally conclude with a brief discussion in Section 5.

2 Methods

2.1 Model Formulation with Connectome Predictors

Assume for subject i (i = 1, ..., n), the brain functional activities are measured under T cognitive states. For state t (t = 1, ..., T), the functional connectome can be summarized by a graph $\mathcal{G}_{it} = (\mathcal{V}_{it}, \mathcal{E}_{it})$ specifying a set of nodes \mathcal{V}_{it} for the brain regions of interest (ROIs), and a set of edges \mathcal{E}_{it} for connections. Under one single brain atlas, all the subjects and states share the same set of ROIs \mathcal{V} with a dimension V. Each functional graph can then be represented by a symmetric connectivity matrix $\mathbf{A}_{it} = (a_{it,kl})$ with its (k,l)th entry $a_{it,kl}$ characterizing the state-specific connectivity between regions k and l. Stacking all the T connectivity matrices, we denote $\mathcal{A}_i \in \mathbb{R}^{V \times V \times T}$ the multi-state functional connectome tensor. To associate these brain functional organizations revealed under different cognitive states to a behavior outcome y_i , we propose the following general connectome-based regression model with individualized effects

$$y_i = \mathbf{x}_i^T \mathbf{\gamma} + f(\mathcal{A}_i, \mathcal{B}_i) + \epsilon_{1i}. \tag{1}$$

Here, $\mathcal{B}_i \in \mathbb{R}^{V \times V \times T}$ is the connectome effect tensor for each subject, which compared with an overall effect summarized over all the subjects, captures personalized relationships between functional connectome over different states and behavior; $f(\cdot, \cdot)$ is a function to be specified to characterize the association between \mathcal{A}_i and y_i , and we also assume heteroscedasticity for

model (1) with $\epsilon_{1i} \sim N(0, \sigma_{1i}^2)$. Finally, in practice, besides imaging features, we also adjust for Q non-image covariates, e.g., age and gender, as denoted by \mathbf{x}_i with the first element to be 1 corresponding to the intercept with their effect characterized by coefficients γ .

There are different options to specify $f(\cdot,\cdot)$ in model (1) in order to parametrize the connectome effect. For instance, the most widely used operation, as it is adopted in the existing connectome-based predictive models (CPMs) (Greene et al., 2018) is to set $f(\cdot, \cdot) = \langle \cdot, \cdot \rangle_F$ with $\langle \cdot, \cdot \rangle_F$ denoting the Frobenius inner product. Such an operation essentially imposes an additive effect among all elements, i.e., $\langle \mathcal{A}_i, \mathcal{B}_i \rangle_F = \sum_{k=0}^{V} \sum_{l=0}^{V} \sum_{k=0}^{T} a_{it,kl} \mathcal{B}_i(k,l,t)$, which is essentially vectorizing the original matrix or tensor with limited consideration on its brain network configuration. As an alternative, in light of the recent discovery that brain functional organization encompasses the cognitive processes through sub-networks (Wig, 2017), we assume the connectome at each state can be partitioned into smaller co-functioning modules through a stochastic block mechanism. Here, instead of directly using the established canonical brain sub-networks (Yeo et al., 2011) which were constructed purely from correlation among fMRI time series, we assume the network parcellations are unknown and will be estimated by our supervised learning procedure to reflect the brain network configuration alternation on behaviors. We also allow the network parcellation to be state-specific in line with the latest discovery in neuroscience that the functional architecture of brain varies by cognitive states (Mennes et al., 2013).

Specifically, let all the brain regions be allocated into M sub-networks at state t. For each node $v \in \mathcal{V}$, we characterize its community membership by a random vector $\mathbf{z}_{vt} = (z_{vt1}, z_{vt2}, \dots, z_{vtM})^T$ with element z_{vtm} being 1 if node v belongs to sub-network m, and 0 otherwise. Conditional on the community membership, we construct a weighted stochastic block model (SBM) for each functional connectivity \mathbf{A}_{it} , i.e., the frontal slice of \mathcal{A}_i , with

individual connectivity element following a conditional normal distribution

$$a_{it,kl} \mid z_{ktm} = 1, z_{ltm'} = 1 \sim N(s_{it,mm'}, \delta^2),$$
 (2)

with mean parameter $s_{it,mm'}$ indicating the expected subject- and state-specific connectivity strength between sub-network m and m', and δ^2 characterizing the variance. We choose a normal distribution given the continuous scale of brain functional connectivity is commonly obtained by applying the Fisher z-transformation on the pairwise Pearson's correlations from the corresponding fMRI time series. It is worth noting that M can be considered as the upper bound of the number of sub-networks across the states. Given different states could have different numbers of sub-networks, when fewer sub-networks are needed to characterize the topological structure under a certain state, not all the pre-booked blocks would be filled in.

Through model (2), we extract the biological topology information of connectomes captured by the community membership tensor $\mathcal{Z} \in \mathbb{R}^{M \times V \times T}$ with its frontal slice $\mathcal{Z}_{:,:,t} = (\boldsymbol{z}_{1t}, \dots, \boldsymbol{z}_{Vt})$, along with the connectivity strength. After dissecting this topological organization information, we summarize the latent sub-network level connectivity strength for subject i by a tensor $\mathcal{S}_i \in \mathbb{R}^{M \times M \times T}$ with each element $\mathcal{S}_i(m, m', t) = s_{it,mm'}$. Through this latent tensor, when assuming $f(\cdot, \cdot)$ to be a Frobenius inner product, the general connectome-based regression model (1) can be re-formulated as

$$y_i = \mathbf{x}_i^T \mathbf{\gamma} + \langle \mathcal{S}_i, \mathcal{W}_i \rangle_F + \epsilon_i, \tag{3}$$

where $W_i \in \mathbb{R}^{M \times M \times T}$ is the corresponding heterogeneous coefficient tensor with element $W_i(m, m', t) = w_{it,mm'}$, and $\epsilon_i \sim (0, \sigma_i^2)$. Different from model (1), the Frobenius inner product is applied plausibly here with the network topology information extracted aside. In Section 1.1 of the Supplementary Material, we show the representation of σ_i^2 and that

 $w_{it,mm'}$ in model (3) is equivalent to $\sum_{k}^{V} \sum_{l}^{V} \mathcal{B}_{i}(k,l,t)$ if $z_{ktm} = 1, z_{ltm'} = 1$. This indicates that $w_{it,mm'}$ aggregates the effects from all the connections between sub-networks m and m' given the unknown community allocations.

2.2 Supervised Heterogeneity Analysis with Feature Selection

Through the individualized parameters in model (3), we hope to facilitate a supervised heterogeneity analysis to group the subjects by brain-to-behavior relationships, and characterize the connectome-based effect mechanism for each subtype. To achieve this, we first denote $\boldsymbol{\theta}_i = \{W_i, \sigma_i\} = \{(w_{it,mm'})_{t=1,\cdots,T,\ 0 < m \le m' \le M}, \sigma_i\}$ the personalized parameter set for subject i, and we assume $\boldsymbol{\theta}_i \sim \mathcal{G}$ which is a joint probability distribution. Specifically, we assume that \mathcal{G} is distributed according to a Dirichlet process, denoted by $\mathcal{DP}(\mathcal{G}_0, \alpha)$, with \mathcal{G}_0 the base measure for the expectation of the random probability and α the scale parameter to describe the variance. To specify the Dirichlet process, we further apply a stick-breaking representation based on a weighted sum of infinite point masses (Sethuraman, 1994) as

$$\mathcal{G} = \sum_{h=1}^{\infty} \vartheta_h \delta(\boldsymbol{\eta}_h), \quad \text{with} \quad \vartheta_h = \nu_h \prod_{d=1}^{h-1} (1 - \nu_d)$$
$$\boldsymbol{\eta}_h \overset{\text{i.i.d}}{\sim} \mathcal{G}_0; \qquad \nu_h \mid \alpha \overset{\text{i.i.d}}{\sim} \text{Beta}(1, \alpha),$$
(4)

where $\delta(\eta_h)$ represents a probability measure concentrated at η_h . Model (4) indicates that \mathcal{G} is almost surely discrete; and its realizations for θ_i are sampled from the component set $\{\eta_h\}_{h=1}^{\infty}$ under weights $\{\vartheta_h\}_{h=1}^{\infty}$ with each of the components independently sampled from base measure \mathcal{G}_0 . Given that the sampling weights decrease exponentially in expectation with h increasing, the sampling items will concentrate on a few initial components of $\{\eta_h\}_{h=1}^{\infty}$. Eventually, the subjects will be grouped into the same subtype when their realizations for the subject-specific parameters θ_i take the identical value; and the number of subtypes will be

automatically reflected. In each subtype, subjects share the same influence of connectivity strength on the outcome, and thus different subtypes vary in effect mechanisms.

Here, the choice of base measure will directly impact the realization for θ_i . Particularly, each $w_{it,mm'}$ characterizes the influence on the outcome by connections between sub-networks m and m' under cognitive state t. Given the neural circuits that relate to certain behavior trait tend to concentrate on specific functional organizations, we anticipate the predictive signals across brain network architecture are sparse with only a few sub-networks under each state associated with the outcome. To distinguish the signal from noise network features, we assign the base measure

$$\mathcal{G}_0 = \prod_{t=1}^T \prod_{m=1}^{M-1} \prod_{m'=m}^M \text{Lap}(\frac{2\sigma^2}{\lambda}) \text{IG}(a_1, b_1),$$
 (5)

with Lap(\cdot) and IG(\cdot , \cdot) representing the Laplace distribution for coefficient $w_{it,mm'}$ and Inverse Gamma distributions for variance σ_i , and λ controlling the degree of shrinkage. The above distribution will induce a simultaneous shrinkage joint with the sub-network construction and subtype establishment, allowing us to define each brain-to-behavior subtype through their unique functional network phenotypes.

Furthermore, we impose priors for the rest of the parameters. For each of the latent connectivity strength and variance, we assign $s_{it,mm'} \sim N(0, \tau^2)$; and assume $\delta^2 \sim IG(a_2, b_2)$. We also impose a noninformative multivariate normal prior for the nuisance parameters $\gamma \sim N(0, I\sigma_0^2)$ where we can set a large value for σ_0^2 in practice. For the random community membership \mathcal{Z} to represent sub-network parcellations, we assign each z_{vt} to follow a multinomial distribution (MN) with M categories and a state-specific probability weight vector $\psi_t = (\psi_{t1}, \dots, \psi_{tM})$, for $v = 1, \dots, V$, $t = 1, \dots, T$. Rather than pre-specifying the allocation weights ψ_t at each state, we choose to assign them a Dirichlet distribution hyper-prior with parameters $g = (g_1, \dots, g_M)$. For the scalar parameter α in the \mathcal{DP} , we

choose a noninformative Gamma hyper-prior G(1,1) to allow enough flexibility for concentration of grouping subjects to subtypes. The whole modeling framework, named Bayesian Connectome-based Heterogeneity Analysis (BCHA), works in an integrative way to characterize the heterogeneous relationship between multi-state connectome predictors and a scale outcome, dissect the brain network topological architecture by constructing sub-networks parcellation, and define each subtype by identifying effective sub-network features.

2.3 Variational Expectation Maximization

We conduct posterior computation for the proposed BCHA. Based on the truncated representation of \mathcal{DP} (Ishwaran and Zarepour, 2000), we choose a conservative value H to cover the upper limit of the number of subtypes, and introduce a latent subtype membership matrix $U = (u_1, \dots, u_n)$ with H dimensional vector u_i for the membership of subject i following a MN distribution under weights $(\vartheta_1, \ldots, \vartheta_H)$, where the weights are fully determined by $\boldsymbol{\nu} = (\nu_1, \dots, \nu_H)$ as shown in (4). The modeling framework of BCHA can be demonstrated by Figure 1. Although it is feasible to develop Markov Chain Monte Carlo (MCMC) algorithms directly from the posterior likelihood, MCMC tends to suffer from poor mixing and prohibitive computation with a large number of unknown parameters. As an alternative, we resort to the variational inference approach, which formulates a variational distribution to approximate the actual posterior distribution. We first consider a variational distribution from the canonical mean-field approximation (Ghahramani and Beal, 2001) and assume that the variational distribution can be partitioned into independent components. However, the Laplace distributions in (5) is elaborated and required additional involvement for the meanfield approximation. Therefore, we develop a variational expectation maximization (VEM) algorithm to employ a more tractable optimization.

Specifically, we denote all the parameters in BCHA as $\Theta = \{ \gamma, \mathcal{Z}, \psi, U, \nu, \delta, (\mathcal{W}_i)_{i=1}^n, \mathcal{U}, \mathcal$

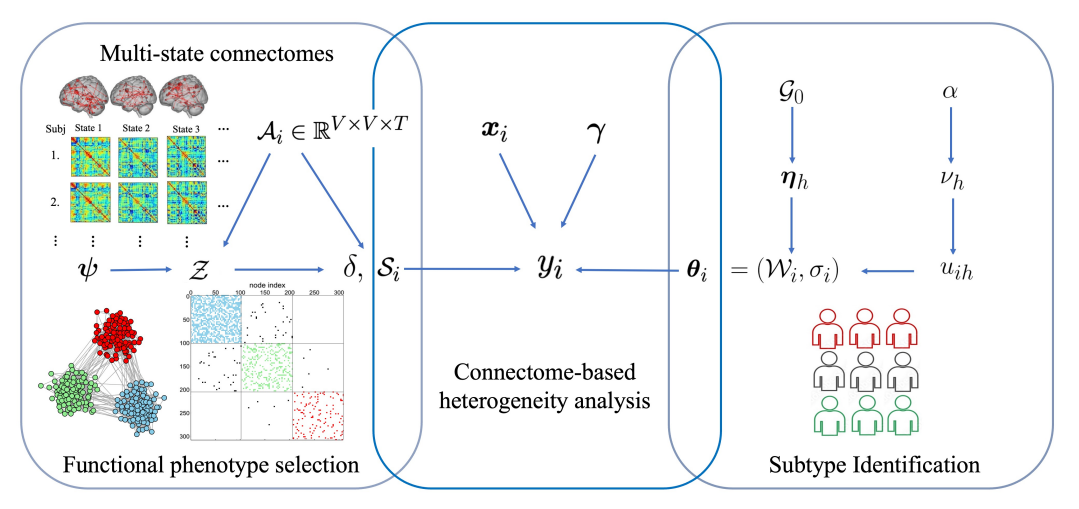


Figure 1: A demonstration of the Bayesian connectome-based heterogeneity analysis (BCHA) modeling framework.

 $(\sigma_i)_{i=1}^n, (\mathcal{S}_i)_{i=1}^n$. The set can be divided into the primary parameters in the regression model $\Theta_M = \{(\mathcal{W}_i)_{i=1}^n, (\sigma_i)_{i=1}^n, \boldsymbol{\gamma}\}$, and the remaining latent parameters $\Theta_L = \{\mathcal{Z}, \boldsymbol{\psi}, \boldsymbol{U}, \boldsymbol{\nu}, \delta, (\mathcal{S}_i)_{i=1}^n\}$. We pursue the maximum a posteriori probability (MAP) estimates for Θ_M by

$$\widehat{\mathbf{\Theta}}_{M} = \underset{\mathbf{\Theta}_{M}}{\operatorname{arg \, max}} \log \pi(\mathbf{\Theta}_{M} \mid \bullet) = \underset{\mathbf{\Theta}_{M}}{\operatorname{arg \, max}} \left\{ \mathcal{L}(\mathbf{\Theta}_{M}) + \log \pi(\mathbf{\Theta}_{M}) \right\}, \tag{6}$$

with \bullet denoting the observed data, $\mathcal{L}(\Theta_M)$ the log-likelihood of observations. For a given distribution $q(\Theta_L)$ for the latent variables, we represent $\mathcal{L}(\Theta_M)$ as (Neal and Hinton, 1998)

$$\mathcal{L}(\Theta_{M}) = \int_{\Theta_{L}} q(\Theta_{L}) \log \pi(\bullet | \Theta_{M}) d\Theta_{L}$$

$$= \int_{\Theta_{L}} q(\Theta_{L}) \log \left(\frac{\pi(\bullet, \Theta_{L} | \Theta_{M})}{q(\Theta_{L})} \right) d\Theta_{L} + \left[- \int_{\Theta_{L}} q(\Theta_{L}) \log \left(\frac{\pi(\Theta_{L} | \bullet, \Theta_{M})}{q(\Theta_{L})} \right) d\Theta_{L} \right].$$
(7)

The second term on the right hand side of (7) is the Kullback-Leibler (KL) divergence between distributions $\pi(\Theta_L|\bullet,\Theta_M)$ and $q(\Theta_L)$. Since KL divergence is non-negative, the first term, known as the evidence lower bound (ELBO), provides the lower bound for $\mathcal{L}(\Theta_M)$. Leveraging the ELBO which is denoted as $F(q, \Theta_M)$, we reconstruct the optimization problem (6) as $\widehat{\Theta}_M = \arg \max_{\Theta_M} \{F(q, \Theta_M) + \log \pi(\Theta_M)\}$. This motivates an EM procedure by iteratively applying the E-step and M-step until convergence. In the following, we briefly explain each step, and relegate more technical details in the Section 1.2 of the Supplementary Materials.

E-step embedded with variational approximation. The E-step is designed to find a distribution $q(\Theta_L)$ that minimizes the KL divergence between $q(\Theta_L)$ and $\pi(\Theta_L|\bullet,\Theta_M)$. Specifically, the posterior distribution can be represented by

$$\pi(\boldsymbol{\Theta}_L \mid \bullet, \boldsymbol{\Theta}_M) \propto \pi \left\{ \boldsymbol{y} \mid \boldsymbol{\Theta}, \boldsymbol{x}, (\mathcal{A}_i)_{i=1}^n \right\} \prod_{i=1}^n \pi(\mathcal{A}_i \mid \boldsymbol{\Theta}) \pi(\mathcal{Z} | \boldsymbol{\psi}) \pi(\boldsymbol{\psi}) \pi(\boldsymbol{U} | \boldsymbol{\nu}) \pi(\boldsymbol{\delta}) \prod_{i=1}^n \pi(\mathcal{S}_i),$$

based on which, we can write down the analytical form of $\pi(\Theta_L|\bullet,\Theta_M)$. Given the complex dependency among the large number of parameters, it is anticipated that a direct posterior sampling will lead to intensive computation and poor mixing. To mitigate this problem, we propose a variational distribution to approximate the above posterior distribution via the mean-field approximation method (Ghahramani and Beal, 2001). To this end, we assume the variational measure $q(\Theta_L)$ can be expressed as a product of independent measures on individual latent variables

$$q(\mathbf{\Theta}_L) = q(\mathbf{Z})q(\boldsymbol{\psi})q(\delta)q(\boldsymbol{U})q(\boldsymbol{\nu})q\left\{(\mathbf{S}_i)_{i=1}^n\right\}. \tag{8}$$

Under variational measure $q(\cdot)$, we consider the realization on \mathcal{Z} , $\boldsymbol{\psi}$, δ , \boldsymbol{U} , $\boldsymbol{\nu}$, and $(\mathcal{S}_i)_{i=1}^n$

coming from an exponential family as

$$\begin{aligned} & \boldsymbol{z}_{vt} \sim \text{MN}(\widetilde{\boldsymbol{\psi}}_{vt}), \quad \widetilde{\boldsymbol{\psi}}_{vt} = (\widetilde{\boldsymbol{\psi}}_{vt1}, \cdots, \widetilde{\boldsymbol{\psi}}_{vtM}), \quad t = 1, \dots, T, v = 1, \cdots, V, \\ & \boldsymbol{\psi}_{t} \sim \text{Dir}(\boldsymbol{\phi}_{t}), \quad \boldsymbol{\phi}_{t} = (\boldsymbol{\phi}_{t1}, \cdots, \boldsymbol{\phi}_{tM}), \quad t = 1, \dots, T, \\ & s_{it,mm'} \sim \text{N}(\boldsymbol{\mu}_{it,mm'}, \boldsymbol{\rho}_{it,mm'}), \quad i = 1, \dots, n, \quad t = 1, \dots, T, \quad m, m' = 1, \dots, M, \\ & \boldsymbol{u}_{i} \sim \text{MN}(\frac{\exp(b_{i1})}{\sum_{h=1}^{H} \exp(b_{ih})}, \cdots, \frac{\exp(b_{iH})}{\sum_{h=1}^{H} \exp(b_{ih})}), \quad i = 1, \dots, n, \\ & \boldsymbol{\nu}_{h} \sim \text{Beta}(f_{h}, O_{h}), \quad h = 1, \dots, H; \quad \text{with } q(\boldsymbol{\nu}_{H} = 1) = 1; \quad \delta^{2} \sim \text{IG}(\boldsymbol{a}_{\delta}, b_{\delta}). \end{aligned}$$

The parameters $\{(\widetilde{\boldsymbol{\psi}}_{vt})_{v=1,\cdots,V,\ t=1,\cdots,T}, (\boldsymbol{\phi}_t)_{t=1,\cdots,T}, (a_{\delta},b_{\delta}), (\mu_{it,mm'},\rho_{it,mm'})_{t=1,\cdots,T,\ 0< m\leq m'\leq M}, (b_{ih})_{i=1,\cdots,n,\ h=1,\cdots,H}, (f_h,O_h)\}$ introduced in the distributions above are the variational parameters. Within the E-step, they can be updated according to a minimization of the KL divergence. For any single parameter within $\boldsymbol{\Theta}_L$, if we generally denote it as κ , then the optimization problem can be achieved by computing $\log q(\kappa) = \mathbb{E}_{\boldsymbol{\Theta}_L \setminus \kappa} \{\log \pi(\bullet, \boldsymbol{\Theta}_L | \boldsymbol{\Theta}_M)\}$ +constant (Tzikas et al., 2008), where $\mathbb{E}_{\boldsymbol{\Theta}_L \setminus \kappa} \{\log \pi(\bullet, \boldsymbol{\Theta}_L | \boldsymbol{\Theta}_M)\}$ is the expectation of the logarithm of the joint probability of the data and latent parameters given $\boldsymbol{\Theta}_M$ taken over all variables except κ , which can be simplified into a function of the fixed parameter $\boldsymbol{\Theta}_M$ and the expectation of remaining parameter set $(\boldsymbol{\Theta}_L \setminus \kappa)$. This creates circular dependencies between the variational parameters from $\boldsymbol{\Theta}_L$ and the expectation of the other latent variables, facilitating a sequential update for the variational parameters. Detailed derivations for variational parameter updating schemes are provided in the Section 1.2 of the Supplementary Materials.

M-step. In M-step, we maximize $F(q, \Theta_M) + \log \pi(\Theta_M)$ with respect to Θ_M . Given the variational parameters, we have $F(q, \Theta_M) = \mathbb{E}_q \{\log \pi(\bullet, \Theta_L | \Theta_M)\} - \mathbb{E}_q \{\log q(\Theta_L)\}$. The optimization procedure then becomes to solve the maximization objective function by updating $(\mathcal{W}_i)_{i=1}^n$, $(\sigma_i^2)_{i=1}^n$ and γ , respectively. We briefly describe the optimization setup for

each parameter, and provide the detailed algorithms in the Section 1.2 of the Supplementary Materials.

Assume subject i has been assigned into subtype h at the current iteration with subtype coefficient tensor denoted as \mathcal{W}_h and random error variance denoted as σ_h . For each subtype h, we use a coordinate descent algorithm to update each element of \mathcal{W}_h , and solve the objective function to update σ_h by the close form as

$$\mathcal{W}_{h} = \arg\min\left[\sum_{i}^{n} \mathbb{E}_{q}(u_{ih})\mathbb{E}_{q}\left\{(y_{i} - \boldsymbol{x}_{i}^{T}\boldsymbol{\gamma} - \langle \mathcal{S}_{i}, \mathcal{W}_{h}\rangle_{F})^{2}\right\} + \lambda \sum_{t}^{T} \sum_{m=1}^{M-1} \sum_{m'=m}^{M} |w_{ht,mm'}|\right].$$

$$\sigma_{h}^{2} = \arg\min\left[\frac{1}{2}\sum_{i}^{n} \mathbb{E}_{q}(u_{ih})\mathbb{E}_{q}\left\{(y_{i} - \boldsymbol{x}_{i}^{T}\boldsymbol{\gamma} - \langle \mathcal{S}_{i}, \mathcal{W}_{h}\rangle_{F})^{2}/\sigma_{h}^{2} + \log\sigma_{h}^{2}\right\}\right]$$

$$+ \frac{1}{2}\sum_{t}^{T} \sum_{m=1}^{M-1} \sum_{m'=m}^{M} (\lambda|w_{ht,mm'}|/\sigma_{h}^{2} + \log\sigma_{h}^{2}) + (a_{1} + 1)\log\sigma_{h}^{2} + b_{1}/\sigma_{h}^{2}\right].$$

Similarly, γ can also be updated by its close form under the objective function γ follows

$$\gamma = \arg\min \left[\sum_{i=1}^{n} \sum_{h=1}^{H} \mathbb{E}_{q}(u_{ih}) \mathbb{E}_{q} \left\{ (y_{i} - \boldsymbol{x}_{i}^{T} \boldsymbol{\gamma} - \langle \mathcal{S}_{i}, \mathcal{W}_{h} \rangle_{F})^{2} / \sigma_{h}^{2} \right\} + \sum_{q}^{Q} (\gamma_{q}^{2} / \sigma_{0}^{2}) \right].$$
(9)

2.4 Numerical characteristics

To guarantee the robustness of the proposed model, the hyper-parameters that needed to be prespecified are assigned values to facilitate noninformative prior supports. The two tuning parameters to be specified are λ to control the sparsity of the selected network features, and M to determine the number of community parcellated across brain regions. There are various strategies one can adopt to select tuning parameters including cross-validation or model selection criteria. Here, to choose the values of (λ, M) , we use variational Bayes Information Criteria (vBIC) (You et al., 2014), a variational Bayes based analogue of Bayesian informa-

tion criterion defined as vBIC = $-2\mathbb{E}_q \log \pi(\bullet|\Theta) + 2\mathbb{E}_q \log q(\Theta)$ with detailed derivations provided in Section 1.2 of the Supplementary Materials. It has been shown that vBIC shares consistent model selection results and first-order asymptotic properties with BIC, and works fine under complex models (You et al., 2014). In our simulations provided in both the main text and Supplementary Materials, we also confirm that it is applicable as an information criterion for our model.

After fitting the model under the current subjects (training set), we can obtain a series of results including the sub-network partition under each cognitive state, constructed subtypes among subjects, and the informative imaging network features along with their effect for each subtype. On the test set, we need to classify each new subject to one of the constructed subtypes. Given our subtypes of interest are defined by the relationship between functional connectome tensor and outcome, the assignment of the subtype for a new observation requires the information on this relationship available from the observed data. Denote the observation for the new subject by $(y_{\text{new}}, \boldsymbol{x}_{\text{new}}, \mathcal{A}_{\text{new}})$. To assign its subtype membership, we compute the sub-network level connectivity strength \mathcal{S}_{new} based on \mathcal{A}_{new} and the estimated \mathcal{Z} ; and calculate the log-likelihood by grouping this new observation to each of the subtypes leveraging the estimate for \mathcal{W}_h and σ_h^2 from the training set by

$$\mathcal{L}_h = -\frac{1}{2} \left\{ (y_{\text{new}} - \boldsymbol{x}_{\text{new}}^T \boldsymbol{\gamma} - \langle \mathcal{S}_{\text{new}}, \mathcal{W}_h \rangle_F)^2 / \sigma_h^2 + \log \sigma_h^2 \right\}, \quad h = 1, \dots, H.$$
 (10)

We then assign this subject to the subtype $h_{\text{new}} \in \{1, \dots, H\}$ with the largest likelihood on (10).

3 Analysis of the ABCD study

We apply our BCHA model to the ABCD data to study the heterogeneous impact of functional connectome on Cognition Fluid Composite Uncorrected Standard Score (FCS), a composite score derived from five measures of fluid abilities (the Dimensional Change Card Sort Test, the Flanker Inhibitory Control and Attention Test, the Picture Sequence Memory Test, the List Sorting Working Memory Test, and the Pattern Comparison Processing Speed Test) (Heaton et al., 2014).

We construct functional connectivity under both resting-state and three cognitive tasks for each participant from raw DICOM image data. The pre-processing is performed in BioImage Suite (Joshi et al., 2011) following the standard steps described in detail elsewhere (Greene et al., 2018; Horien et al., 2019; Rapuano et al., 2020). All fMRI images are realigned to correct for motion, registered to MNI space, and anatomically parcellated using a 268-node whole-brain atlas (Shen et al., 2013). Covariates of no interest are regressed from the data, including linear, quadratic, and cubic drifts, 24-motion parameters (Satterthwaite et al., 2013), mean cerebral-spinal fluid signal, mean white matter signal, and overall global signal. Data are temporally smoothed with a Gaussian filter, $\sigma=1.95$ (approximate cut-off frequency of 0.12 Hz). Pearson correlation coefficients between time courses for every pair of nodes are computed and Fisher z-transformed, resulting in a 268×268 functional connectivity matrix for each state and each participant. For task-based fMRI, we include participants with mean framewise displacement (FD) under a motion threshold of 0.1 mm (Greene et al., 2018; Stark et al., 2021). For resting-state fMRI, we include one resting-state run for each participant in the analyses. To maximize sample size, participants with at least one resting-state scan with mean FD under the 0.1 mm threshold are included. For participants who have more than one run with mean FD under the 0.1 mm threshold, we select the run with the lowest mean FD for use in the analyses. After additionally excluding those with low quality anatomical images by FreeSurfer (ABCD NDA name: fsqc_qc), the number of remaining participants under each state is 2,581 for the resting-state; 1,543 for the MID task; 1,553 for the SST; and 1,465 for the EN-back task.

To guarantee a reasonable sample size and accommodate the complementary information among states, we consider integrating functional connectome under two states at a time, i.e. Resting & MID, Resting & EN-back, and MID & EN-back. To avoid introducing unnecessary noise, we exclude SST from the current analysis given that it results in relevantly low predictive accuracy compared with the other states in our preliminary analysis (please refer to the Section 2.1 of the Supplementary Materials for more details). For each set of analyses, we adjust for age, sex, and race (white vs. others); and remove siblings to avoid confounders associated with family relatedness. These result in 1,208, 1,126 and 944 participants included in the above three sets of functional connectivity combinations, respectively; and their demographic information is shown in the Section 2.2 of the Supplementary Materials. To implement BCHA, we set hyper-parameters $a_k = b_k = 10 \ (k = 1, 2), \ \sigma_0^2 = 10, \ \tau = 1, \ \text{and}$ $g_m=1, m=1,\ldots,M$ to induce noninformation priors. We examine $\lambda=(10^{-3},10^{-4},10^{-5})$ and the upper limit of number of sub-networks M = (2, 3, 4, 5, 6, 7). We select the best value of (λ, M) using vBIC as described in Section 2.4. To account for potential demographic and socio-economic selection bias in the national sampling and recruitment, we incorporate a propensity score (Heeringa and Berglund, 2020) for each child in the ABCD study as weights in our regression models. Finally, we summarize the computational cost in the Section 2.3 of the Supplementary Materials to show our computational efficiency.

3.1 Subtype and sub-network construction

To determine the sub-networks developed at each state and eventual supervised subtypes, we combine training and testing sets and reapply BCHA to the three sets of state combinations.

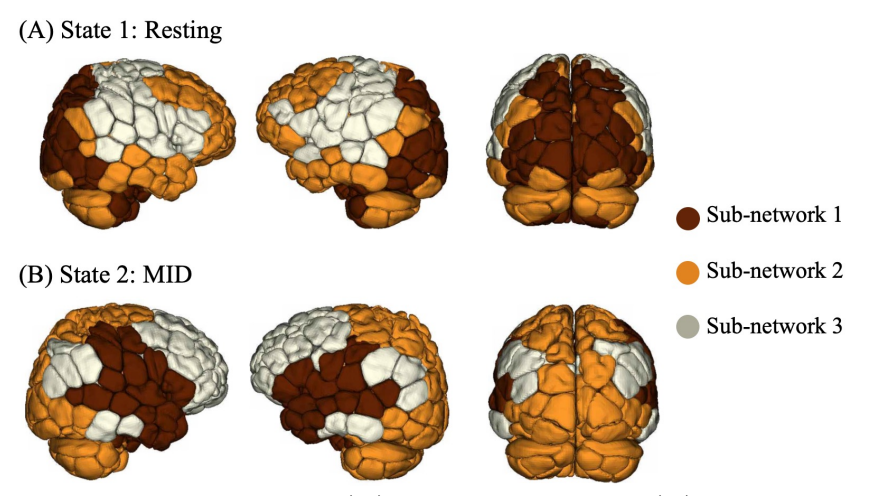


Figure 2: Sub-network partition under (A) Resting-state and (B) Monetary incentive delay (MID) task.

Here, we only present the results from integrating functional connectomes under Resting & MID, and refer to the Section 2.5 of the Supplementary Materials for the remaining results.

After determining the tuning parameters by vBIC, we partition the ROIs under each state into three sub-networks. The sub-networks consist of 101, 93, and 74 regions under resting-state, and 131, 87, and 50 regions under MID. Figure 2 shows the sub-networks under two states. Based on the figure, the sub-network allocation is highly symmetric between the left and right hemispheres, which is biologically plausible given the similar neuronal activity patterns. Under different states, the sub-network partitions are distinct, which is consistent with previous studies that functional architectures are not identical during different cognitive states (Mennes et al., 2013). Of note, there are also three sub-networks determined under resting-& EN-back-state (Section 2.5.3 of the Supplementary Materials); and we observe a highly consistent resting-state partition, indicating the robustness of our analyses. Finally, we compare our constructed sub-networks with the canonical sub-networks defined under resting-state, and summarize the result in the Section 2.5.2 of the Supplementary Materials.

In terms of subtypes, our analyses define seven unique subtypes to reflect heterogeneous predictive mechanisms. Table 1 shows the demographic information and FCS for each subtype by ordering the subtype index by the average FCS. Based on the results, we conclude that participants from different subtypes significantly differ in race, age, and FCS; and subtypes composed of younger children have higher FCS, and those with the lowest or highest FCS have a lower percentage of white compared to the rest. We then compare the connectivity strength among subtypes. In general, we observe the overall connectivity is positive within sub-networks and negative between them. As for the impact of sub-network connec-

Table 1: Demographic information and fluid composite uncorrected standard score (FCS) for seven subtypes

Characteristics	Subtype 1	Subtype 2	Subtype 3	Subtype 4	Subtype 5
	(N=92)	(N=132)	(N=137)	(N=336)	(N=171)
Female, No. (%)	49 (53.2)	68 (51.5)	66 (48.2)	178 (52.9)	104 (60.8)
White, No. (%)	54 (58.6)	102 (77.3)	$101\ (73.7)$	257 (76.5)	129(75.5)
Age, mean (sd), months	122.4 (6.9)	122.6 (7.1)	120.7(7.7)	120.4(7.0)	120.19(7.2)
FCS, mean (sd)	78.8(6.1)	85.9(4.1)	88.9(4.6)	93.9(4.5)	98.8(4.4)
	Subtype 6	Subtype 7		Statistics	P value
	(N=173)	(N=167)			
Female, No. (%)	91 (52.6)	77 (46.1)		$\chi^2 = 8.6$	0.19
White, No. (%)	120 (69.4)	110 (65.8)		$\chi^2 = 18.2$	0.005
Age, mean (sd), months	$119.1\ (7.1)$	118.2 (6.6)		F = 6.8	3.5e-7
FCS, mean (sd)	101.8 (5.4)	$107.31\ (5.3)$		F = 529.3	< 2.2e-16

tivity on FCS, we conclude that different subtypes are defined by different network features, and we visualize these informative connections for each subtype in Figure 3 after pruning weak connectivity. More details are described in the Section 2.4 of the Supplementary Materials.

Under resting state, connectivity within three sub-networks are selected by the majority of subtypes, indicating that all the sub-networks have a joint influence on the FCS. In particular, Sub-network 3 is selected by all subtypes, suggesting its importance for FCS

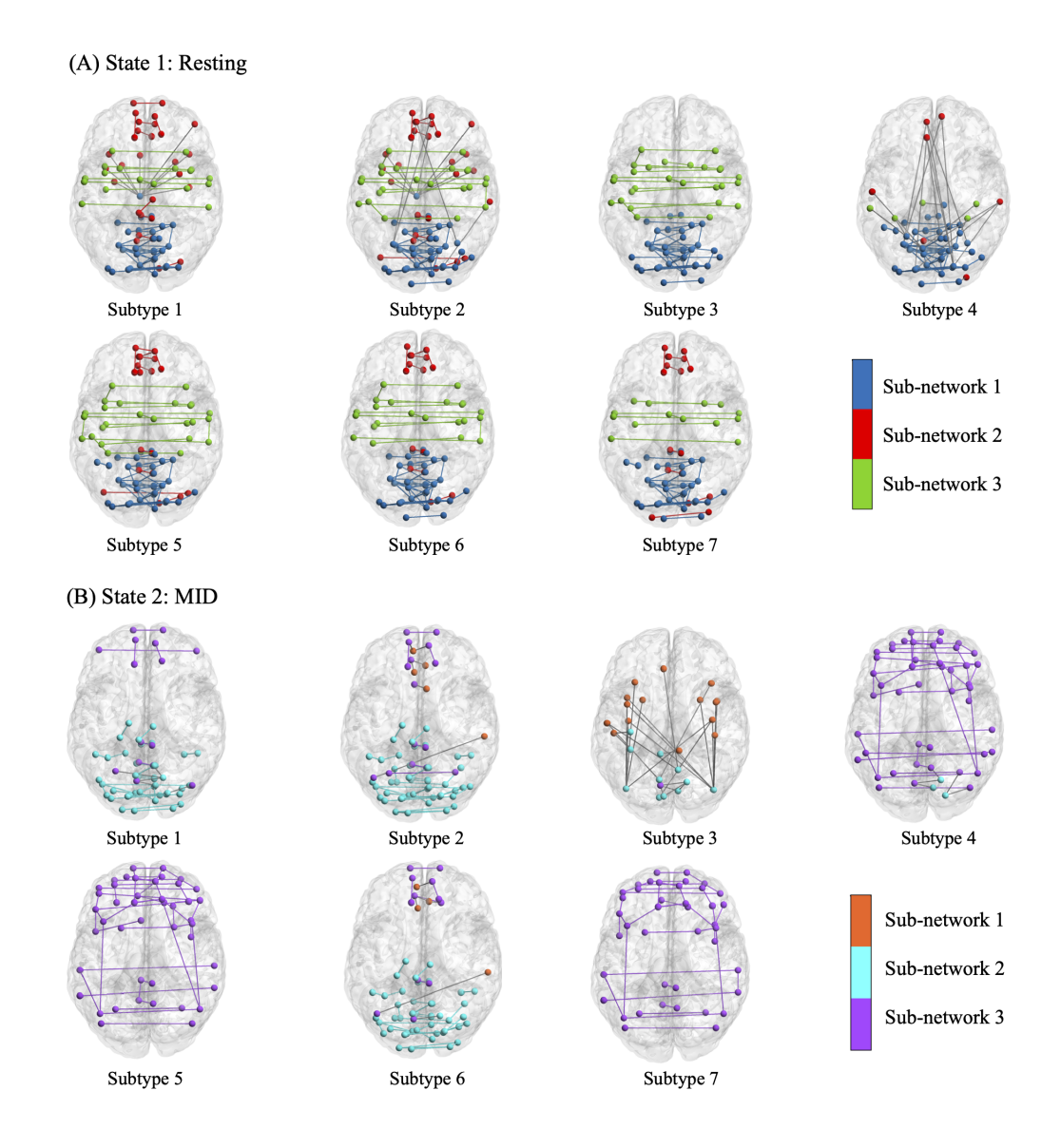


Figure 3: Brian nodes and connectivity edges in selected sub-networks for seven subtypes under (A) Resting-state and (B) Monetary incentive delay (MID) task. Brain nodes within each sub-network are indicated by color. Edges for within-network connectivity are in the same color as brain nodes, and edges for between-network connectivity are in gray color. Edges with weak connectivity strength are pruned for better visualization.

prediction. The between-network connectivity of Sub-networks 1 and 2, and Sub-networks 1 and 3 are selected by several subtypes. The interaction between these sub-networks may contribute to the difference among subtypes. Under MID, connectivity within Sub-network 3 is selected by six subtypes; and connectivity between Sub-networks 3 and 1, and Sub-networks 3 and 2 is also selected by five subtypes, implying Sub-network 3 is a hub sub-network to impact FCS.

Under MID, Sub-network 3 mainly overlaps with the Fronto-parietal Network (FPN, 54%), Medial Frontal Network (16%), and Default Mode Network (DMN, 19%). Notably, it covers 27 (79.4%) brain regions out of all the 34 regions belonging to the FPN (Section 2.5.2) of the Supplementary Materials). The FPN, also known as the central executive network (CEN), is a large-scale brain network involved in a variety of cognitive functions such as working memory, attention, shifting, and reasoning (Niendam et al., 2012). Evidence has shown that FPN serves as a flexible hub of cognitive control (Marek and Dosenbach, 2018). Fluid intelligence is reported to be correlated with across-network connectivity of FPN (Cole et al., 2015) including the functional connectivity between the FPN and DMN (Hearne et al., 2016), which is consistent with our current results. The within-network connectivity of Subnetwork 3 defined in the current study reflects the between-network connectivity of the DMN and FPN given that those canonical sub-networks are grouped into the single Sub-network 3 due to their relatively coherent effects on the FCS. When dealing with high cognitive control, the functional connectivity in the FPN increases and provides an indication of complex task performance (Cole et al., 2012). This may explain why the FPN shows a greater impact on fluid intelligence under MID rather than resting-state in our study.

Sub-network 3 under resting-state mainly overlaps with the Motor Network (50%), Basal Ganglia (16.2%), and Limbic Network (14.8%). Studies have shown that basal ganglia is involved in motor control and multiple cognitive functions, such as executive functions and motivation (Leisman and Melillo, 2013). Basal Ganglia also closely interacts with the Limbic

Network (Aoki et al., 2019) and frontal cortex where most of the regions within the Motor Network are located (Alexander et al., 1986). These findings show a strong consistency with existing neuroscience literature and pave a way to reveal neurobiological mechanisms underlying cognition processes for children in the early adolescence.

4 Simulation studies

To confirm the superior performance of the BCHA, we conduct a series of simulations to support the application in Section 3. We utilize multi-state functional connectivity directly from the ABCD study by randomly sampling 1,000 subjects for their Resting & EN-back functional connectome data. This results in V = 268 and T = 2. We assume the number of sub-networks under each state M=3 with the community allocation directly imported from our data analysis results for Resting & EN-back as presented in the Section 2.5.3 of the Supplementary Materials. This leads to sub-networks consisting of 102, 91, and 75 regions under resting-state, and those consisting of 127, 62, and 79 regions under ENback. We simulate the outcome y in various scenarios considering both homogeneous and heterogeneous brain-to-behavior relationships. In the homogeneous scenario, all the subjects belong to one subtype; and in the heterogeneous scenario, we consider two subtypes and randomly assign subjects to one of them with an equal probability. Then, we assign subtypespecific effect size $\mathcal{W}_h = (w_{ht,mm'})_{t=1,\cdots,T,\ 0 < m \leq m' \leq M}$ to each sub-network under each state. We set $\mathcal{B}_h(k,l,t) = w_{ht,mm'}$ given $z_{ktm} = 1$, $z_{ltm'} = 1$. For each subject i, the outcome y_i is generated based on (1) under its corresponding coefficient tensor with a Frobenius inner product.

We then consider the following three signal settings for the effects:

• Signal 1 (homogeneous): We assume the connections within two of the sub-networks under each state impact the outcome with $w_{11,11} = 0.005$, $w_{11,22} = 0.01$, $w_{12,22} = 0.01$

- 0.01, $w_{12,33} = 0.01$, and the rest elements equal to zero. We set $\sigma_1 = 1.5$.
- Signal 2 (heterogeneous): On the basis of Signal 1, two subtypes vary by effect directions and variance with $w_{11,11} = 0.005$, $w_{21,11} = -0.005$, $w_{12,33} = 0.01$, $w_{22,33} = -0.01$, $w_{11,22} = w_{21,22} = 0.01$, $w_{12,22} = w_{22,22} = 0.01$, and the rest elements equal to zero. We set $\sigma_1 = 2$, $\sigma_2 = 1.5$.
- Signal 3 (heterogeneous): On the basis of Signal 2, we consider more complex signals by including the effects of between-network connectivity. We add $w_{11,31} = 0.005$, $w_{21,31} = 0.01$, and $w_{12,32} = w_{22,32} = -0.05$ to Signal 2. The value of remaining effect and variance are kept the same as the Signal 2.

We compare BCHA with competing alternatives. For each simulated dataset, we split it into a training and testing set with an equal size, and replicate this simulation process 100 times. Besides BCHA, we implement a) two classical high dimensional predictive models—LASSO (Tibshirani, 1996) and Bayesian variable selection with Horseshoe prior (BVSH) (Carvalho et al., 2010) by directly vectorizing the connectivity matrices; b) sparse tensor regression (STR) (Zhou et al., 2013), which directly uses connectivity matrices as predictors; and c) ridge CPM (rCPM) (Gao et al., 2019), a widely used connectome-based predictive model in neuroscience. The LASSO and BVSH are implemented using R packages glmnet and horseshoe; and the STR and rCPM are implemented using Matlab toolboxes TensorReg (https://hua-zhou.github.io/TensorReg/) and CPM (https://github.com/YaleMRRC/CPM), respectively.

There are also tuning parameters involved in the above models that can substantially impact the result, and we have tried to maintain a fair comparison by carefully choosing their values. Specifically, in BCHA, we fix the number of sub-networks M=3 and use vBIC to select λ from (10⁻³, 10⁻⁴, 10⁻⁵). In both LASSO and rCPM, one tuning parameter is involved to control sparsity; and to be consistent with our approach, we select its best value by BIC.

For STR, there are two tuning parameters: r specifying the rank for tensor decomposition and λ controlling the sparsity. Similarly, under grids r = (1, 2, 3) and $\lambda = (0.1, 1, 10, 100)$, we search the best values that lead to the smallest BIC. Here, STR is not directly applicable to our connectome data with a symmetric constraint. Therefore, we summarize its estimation for each coefficient matrix at state t by $\{\mathcal{B}(:,:,t) + \mathcal{B}'(:,:,t)\}/2$ based on its coefficient tensor \mathcal{B} . The posterior inference for BVSH is based on 5,000 iterations of MCMC sampling with the first 2,000 as burn-in. Furthermore, we also include two variations of BCHA by first assuming a homogeneous brain-to-behavior impact without the supervised grouping (BCHA_{homo}); and keeping the same training process as BCHA but randomly assigning the subtype membership for subjects on the testing set without using the log-likelihood criterion described in Section 2.4 (BCHA_{rand}).

We first evaluate the performance of BCHA and its two variations BCHA_{homo} and BCHA_{rand} in terms of the sub-network partition and subtype identification accuracy. These are unique features of our proposed methods. We measure the sub-network partition under each state using adjusted rank index (ARI) (Hubert and Arabie, 1985), which quantifies the similarity between two clustering results. When characterizing the performance of subtype identification, we compute the percentage agreement (PA) as the percentage of subjects with their subtypes correctly aligned.

We compare the accuracy in the parameter estimation and feature selection among all methods. In terms of the parameter estimation, the estimation for LASSO, BVSH, rCPM, and STR are based on individual edge, while that for BCHA is based on sub-networks. To facilitate a fair comparison, given $w_{it,mm'} = \sum \mathcal{B}_i(k,l,t)$ with $z_{ktm} = 1, z_{ltm'} = 1$ as shown in Section 2.1, we accommodate the edge-based methods by mapping the sub-network level parameters estimated under BCHA to its associated edges enforcing each edge with an identical contribution within a sub-network unit to prediction. Then the estimation is assessed by the mean square error (MSE) across all the edges, and can be directly obtained

from the competing edge-based methods. Finally, the feature selection accuracy is assessed by receiver operating characteristic (ROC). To ensure the consistency of the process for all the methods, we calculate the sensitivity and specificity by comparing a re-scaled edge-wise absolute effect size $|\mathcal{B}_i(k,l,t)|/\max|\mathcal{B}_i(k,l,t)|$ with a gradually increased cutoff to determine the signal and noise edges. The average sensitivity and specificity at each cutoff across 100 replications are used to draw the ROC curve.

We first present the sub-network partition under two states and subtype identification results in Table 2. BCHA_{rand} and BCHA differ in the subtype assignment on the testing set only, so they share the sub-network partition. Thus, the ARIs for BCHA_{rand} are not presented in Table 2. BCHA outperforms BCHA_{homo} or achieves the same partition accuracy in both homogeneous and heterogeneous scenarios. Although BCHA's performance shows slight deterioration in Signal 3 in which both the within- and between-network connectivity influence the outcome compared with Signal 2, BCHA manages to dissect the underlying brain sub-network structure with high accuracy.

With respect to subtype identification, since BCHA_{homo} assumes all the subjects belong to one group (PA=1 in Signal 1 and PA \approx 0.5 in Signals 2 and 3), we only compare the results for BCHA and BCHA_{rand}. Specifically, BCHA exhibits better performance than BCHA_{rand} in all signal settings, especially in the heterogeneous scenario. This is expected given BCHA groups subjects to one subtype in the homogeneous scenario and divides them into different subtypes in the heterogeneous scenario. Thus, BCHA_{rand} has similar performance to BCHA in the homogeneous scenario and PA around 0.5 in the heterogeneous scenario. These results demonstrate that BCHA can detect the homogeneous or heterogeneous brain-to-behavior relationship in all signal settings and accurately determine the subtype allocation for subjects on the testing set based on the log-likelihood criterion in (10).

Figure 4 illustrates the performance of parameter estimation and feature selection for all methods. Overall, the proposed BCHA outperforms alternative methods in all signal

Table 2: Adjusted rank index (ARI) of sub-network partition and percentage agreement (AP) of subtype identification over 100 times replication. Q1: 1st quantile; Q3: 3rd quantile.

Signal	Scenario	Method	State 1 ARI	State 2 ARI	PA
8			(Q1 Median Q3)	(Q1 Median Q3)	(sd)
1	Homogeneous	BCHA	0.76 0.89 0.94	0.61 0.93 0.97	0.97(0.04)
		$\mathrm{BCHA}_{\mathrm{homo}}$	0.76 0.88 0.94	0.33 0.88 0.96	_
		$\mathrm{BCHA}_{\mathrm{rand}}$	_	_	0.81 (0.24)
2	Heterogeneous	BCHA	0.89 0.90 0.93	0.93 0.95 0.98	0.87 (0.06)
		$\mathrm{BCHA}_{\mathrm{homo}}$	0.89 0.90 0.96	0.51 0.94 0.96	_
		$\mathrm{BCHA}_{\mathrm{rand}}$	_	_	0.52 (0.01)
3	Heterogeneous	BCHA	0.80 0.84 0.94	0.34 0.86 0.96	0.93 (0.04)
		$\mathrm{BCHA}_{\mathrm{homo}}$	0.70 0.90 0.93	0.33 0.52 0.94	_
		$\mathrm{BCHA}_{\mathrm{rand}}$			0.52 (0.01)

settings. Regarding parameter estimation (Figures 4A), BCHA and BCHA_{homo} consistently achieve lower MSE in all signal settings. However, BVSH and STR exhibit relatively high MSE. With respect to feature selection (Figure 4B), BVSH is slightly inferior to BCHA_{homo} in the homogeneous scenario but substantially outperforms it in the heterogeneous scenario. In Signal 3, the area under the curve (AUC) of BCHA shows deterioration, but it remains the winner of feature selection. RCPM achieves larger AUC than LASSO, BVSH, and STR in the homogeneous scenario, and their AUCs are all close to 0.5 in the heterogeneous scenarios.

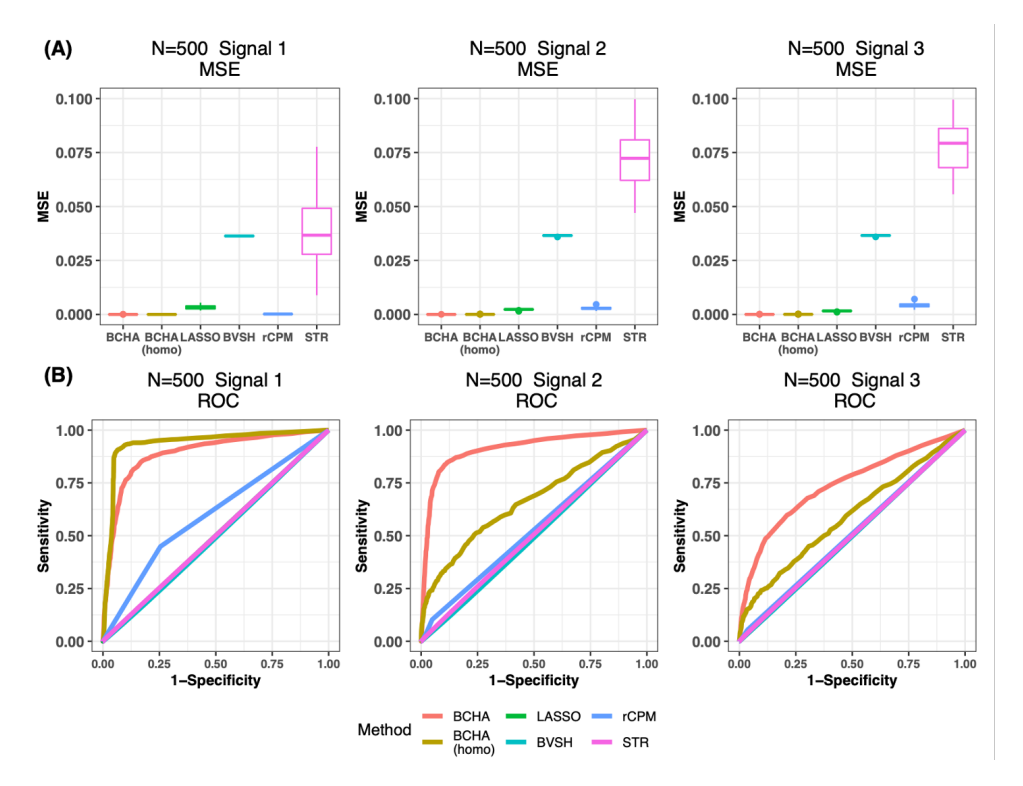


Figure 4: Results of Simulation Study(A) Boxplots of the mean square error (MSE) of parameter estimation. (B) Average ROC curves of feature selection across 100 times replication.

We also perform additional simulation studies by generating functional connectome data with number of ROIs V=100 under the assumption of SBM, simulating outcome values in various signal settings, and examining the impact of sample size (n=200,600,1000) and variance level (low, high) on performance. BCHA achieves high accuracy of sub-network partition and subtype identification and outperforms competing methods in terms of parameter estimation and feature selection even with small sample size and high variance level. Furthermore, we also evaluate the performance of BCHA in simulation settings with a larger number of subtypes, a larger number of subnetworks, and different sub-network numbers across states as provided in the Section 3 of the Supplementary Materials. In all of these simulations, BCHA achieves satisfactory performance in terms of sub-network partition,

subtype identification, parameter estimation, and feature selection, which affirms its broad feasibility.

5 Discussion

In this article, we introduce a novel Bayesian approach named BCHA to associate multistate brain functional connectivity with a behavior outcome. We take into consideration the potential heterogeneity while characterizing the brain-to-behavior relationship. This allows us to uncover subtypes with distinct effect mechanisms. Within the modeling framework, we integrate functional connectivity under both resting-state and cognitive tasks as network predictors and facilitate the dissection of brain network topological architecture under each state. In the application to the multi-state functional connectome in ABCD study, we identify three distinct sub-networks under resting-state and MID, respectively, and define seven subtypes among children in their early adolescence to reflect heterogeneous effect mechanisms. Our results reveal the important role of sub-networks overlapping with Fronto-parietal Network, Medial Frontal Network, and Default Mode Network under MID and sub-networks overlapping with Motor Network, Basal Ganglia, and Limbic Network under resting-state to impact fluid intelligence development, which is consistent with existing neuroscience literature. We also confirm the superiority of BCHA through extensive simulations.

Our analysis suggests distinct sub-network structures under resting- and task-states. Compared to canonical sub-networks defined under resting-state (Yeo et al., 2011), the state-specific brain network topology provides great insight into brain's organization alternating between cognitive states. In the current application, the number of constructed sub-networks is smaller than the canonical sub-networks because our constructed sub-networks reflect the co-functioning of brain network components with respect to a behavior outcome like the FCS. Meanwhile, we select predictive sub-network features for the behavioral outcome,

which may help direct future intervention strategies. More importantly, the heterogeneity analysis defines plausible neurodevelopmental subtypes for children in their adolescence. The characterization of personalized brain-to-behavior effect paradigms reveals potential neurobiological mechanisms underlying human cognition processes during adolescence, an active neurodevelopmental stage. Of note, the seven subtypes identified in this study among children from ABCD study are associated with sociodemographic variables (e.g., race). Given it remains unclear whether these defined subtypes reflect inherent biological differences across races that are relevant to intelligence or whether they capture the effects of adverse environments on intelligence within specific racial groups, further investigation into the underlying mechanisms linking brain functional alterations and behavior traits under different sociodemographic characteristics is a promising avenue for future research.

For model estimation, we develop an efficient VEM algorithm. However, the computation of MAP does not enable the quantification of the uncertainty for parameters $\Theta_M = \{(W_i)_{i=1}^n, (\sigma_i)_{i=1}^n, \gamma\}$. To overcome this limitation of inference, we can compute bootstrap confidence intervals by repeatedly fitting the model to multiple bootstrap samples. In the current model, we choose Laplace distribution as a shrinkage prior for feature selection. An alternative is using a spike-and-slab prior to enable a direct selection of features, but the corresponding algorithm may be more computationally intensive. Currently, we consider the additive effect of connectivity strength on the outcome trait in model 3. An interesting extension is to replace Frobenius inner product with other functions to account for more complex non-linear relationships between connectivity and outcome. For instance, a piecewise linear function for connectivity strength of each edge can be considered under the assumption that the effect of connectivity on the outcome differ by strength level. In this study, we use a stringent threshold of mean FD < 0.1 mm for motion correction following the existing literature. Given the high movement during the scanning for young children, we end up with excluding a large number of subjects that might lead to selection bias (Cosgrove et al., 2022; Nebel et al., 2022). Therefore, a potential next step is to apply the proposed method to a larger cohort say UK Biobank. Some other extensions of our current analysis include to integrate brain connectivity measured by different imaging techniques such as a joint analysis for functional connectivity with structural connectivity summarized by diffusion tensor imaging. We can also consider an integration of both brain connectivity and regional features to enhance prediction from different topological aspects.

Supplementary Materials

The supplementary materials contain detailed derivation on the VEM algorithm and posterior computation steps, additional results of real data analysis, computational time, additional simulations, and R codes to implement the method.

Funding

Zhang's research is partially supported by NIH grants R01HG010171 and R01MH116527 and NSF grant DMS-2112711. Zhao's research is partially supported by NIH grants RF1AG081413, R01EB034720 and RF1AG068191.

Acknowledgment

The authors would like to thank the Editor, the Associate Editor and three anonymous Reviewers for their constructive comments and suggestions which significantly helped improve this paper. Data used in the preparation of this article were obtained from the Adolescent Brain Cognitive Development (ABCD) Study (https://abcdstudy.org), held in the NIMH Data Archive (NDA). This is a multisite, longitudinal study designed to recruit more

than 10,000 children age 9-10 and follow them over 10 years into early adulthood. The ABCD Study is supported by the National Institutes of Health and additional federal partners under award numbers U01DA041048, U01DA050989, U01DA051016, U01DA041022, U01DA051018, U01DA051037, U01DA050987, U01DA041174, U01DA041106, U01DA041117, U01DA041028, U01DA041134, U01DA050988, U01DA051039, U01DA041156, U01DA041025, U01DA041120, U01DA051038, U01DA041148, U01DA041093, U01DA041089, U24DA041123, U24DA041147. A full list of supporters is available at https://abcdstudy.org/federal-partners.html. A listing of participating sites and a complete listing of the study investigators can be found at https://abcdstudy.org/consortium_members/. ABCD consortium investigators designed and implemented the study and/or provided data but did not necessarily participate in the analysis or writing of this report. This manuscript reflects the views of the authors and may not reflect the opinions or views of the NIH or ABCD consortium investigators. We thank the Yale Center for Research Computing for guidance and use of the research computing infrastructure.

References

- Alexander, G. E., DeLong, M. R., and Strick, P. L. (1986), "Parallel organization of functionally segregated circuits linking basal ganglia and cortex," *Annual review of neuroscience*, 9, 357–381.
- Aoki, S., Smith, J. B., Li, H., Yan, X., Igarashi, M., Coulon, P., Wickens, J. R., Ruigrok, T. J., and Jin, X. (2019), "An open cortico-basal ganglia loop allows limbic control over motor output via the nigrothalamic pathway," *Elife*, 8, e49995.
- Arain, M., Haque, M., Johal, L., Mathur, P., Nel, W., Rais, A., Sandhu, R., and Sharma, S. (2013), "Maturation of the adolescent brain," *Neuropsychiatric disease and treatment*, 9, 449.
- Berger, J. O., Wang, X., and Shen, L. (2014), "A Bayesian approach to subgroup identification," *Journal of biopharmaceutical statistics*, 24, 110–129.

- Blakemore, S.-J. (2012), "Imaging brain development: the adolescent brain," *Neuroimage*, 61, 397–406.
- Carvalho, C. M., Polson, N. G., and Scott, J. G. (2010), "The horseshoe estimator for sparse signals," *Biometrika*, 97, 465–480.
- Casey, B., Cannonier, T., Conley, M. I., Cohen, A. O., Barch, D. M., Heitzeg, M. M., Soules, M. E., Teslovich, T., Dellarco, D. V., Garavan, H., et al. (2018), "The adolescent brain cognitive development (ABCD) study: imaging acquisition across 21 sites," *Developmental cognitive neuroscience*, 32, 43–54.
- Cohen, J. R. and D'Esposito, M. (2016), "The segregation and integration of distinct brain networks and their relationship to cognition," *Journal of Neuroscience*, 36, 12083–12094.
- Cole, M. W., Ito, T., and Braver, T. S. (2015), "Lateral prefrontal cortex contributes to fluid intelligence through multinetwork connectivity," *Brain connectivity*, 5, 497–504.
- Cole, M. W., Yarkoni, T., Repovš, G., Anticevic, A., and Braver, T. S. (2012), "Global connectivity of prefrontal cortex predicts cognitive control and intelligence," *Journal of Neuroscience*, 32, 8988–8999.
- Cosgrove, K. T., McDermott, T. J., White, E. J., Mosconi, M. W., Thompson, W. K., Paulus, M. P., Cardenas-Iniguez, C., and Aupperle, R. L. (2022), "Limits to the generalizability of resting-state functional magnetic resonance imaging studies of youth: an examination of ABCD Study® baseline data," *Brain imaging and behavior*, 16, 1919–1925.
- Fox, M. D. and Raichle, M. E. (2007), "Spontaneous fluctuations in brain activity observed with functional magnetic resonance imaging," *Nature reviews neuroscience*, 8, 700–711.
- Friston, K., Frith, C., Liddle, P., and Frackowiak, R. (1993), "Functional connectivity: the principal-component analysis of large (PET) data sets," *Journal of Cerebral Blood Flow & Metabolism*, 13, 5–14.
- Fruhwirth-Schnatter, S., Celeux, G., and Robert, C. P. (2019), *Handbook of mixture analysis*, CRC press.
- Gao, S., Greene, A. S., Constable, R. T., and Scheinost, D. (2019), "Combining multiple connectomes improves predictive modeling of phenotypic measures," *Neuroimage*, 201, 116038.
- Garavan, H., Bartsch, H., Conway, K., Decastro, A., Goldstein, R., Heeringa, S., Jernigan, T., Potter, A., Thompson, W., and Zahs, D. (2018), "Recruiting the ABCD sample: Design considerations and procedures," *Developmental cognitive neuroscience*, 32, 16–22.

- Ghahramani, Z. and Beal, M. J. (2001), "Propagation algorithms for variational Bayesian learning," Advances in neural information processing systems, 507–513.
- Gonzalez-Castillo, J. and Bandettini, P. A. (2018), "Task-based dynamic functional connectivity: Recent findings and open questions," *Neuroimage*, 180, 526–533.
- Greene, A. S., Gao, S., Scheinost, D., and Constable, R. T. (2018), "Task-induced brain state manipulation improves prediction of individual traits," *Nature communications*, 9, 1–13.
- Hagler Jr, D. J., Hatton, S., Cornejo, M. D., Makowski, C., Fair, D. A., Dick, A. S., Sutherland, M. T., Casey, B., Barch, D. M., Harms, M. P., et al. (2019), "Image processing and analysis methods for the Adolescent Brain Cognitive Development Study," *Neuroimage*, 202, 116091.
- Hearne, L. J., Mattingley, J. B., and Cocchi, L. (2016), "Functional brain networks related to individual differences in human intelligence at rest," *Scientific reports*, 6, 1–8.
- Heaton, R. K., Akshoomoff, N., Tulsky, D., Mungas, D., Weintraub, S., Dikmen, S., Beaumont, J., Casaletto, K. B., Conway, K., Slotkin, J., et al. (2014), "Reliability and validity of composite scores from the NIH Toolbox Cognition Battery in adults," *Journal of the International Neuropsychological Society*, 20, 588–598.
- Heeringa, S. G. and Berglund, P. A. (2020), "A guide for population-based analysis of the Adolescent Brain Cognitive Development (ABCD) Study baseline data," *BioRxiv*.
- Horien, C., Shen, X., Scheinost, D., and Constable, R. T. (2019), "The individual functional connectome is unique and stable over months to years," *Neuroimage*, 189, 676–687.
- Hubert, L. and Arabie, P. (1985), "Comparing partitions," *Journal of classification*, 2, 193–218.
- Im, Y., Huang, Y., Tan, A., and Ma, S. (2021), "Bayesian finite mixture of regression analysis for cancer based on histopathological imaging—environment interactions," *Biostatistics*.
- Ishwaran, H. and Zarepour, M. (2000), "Markov chain Monte Carlo in approximate Dirichlet and beta two-parameter process hierarchical models," *Biometrika*, 87, 371–390.
- Joshi, A., Scheinost, D., Okuda, H., Belhachemi, D., Murphy, I., Staib, L. H., and Papademetris, X. (2011), "Unified framework for development, deployment and robust testing of neuroimaging algorithms," *Neuroinformatics*, 9, 69–84.
- Karcher, N. R. and Barch, D. M. (2021), "The ABCD study: understanding the development of risk for mental and physical health outcomes," *Neuropsychopharmacology*, 46, 131–142.

- Leisman, G. and Melillo, R. (2013), "The basal ganglia: motor and cognitive relationships in a clinical neurobehavioral context," *Reviews in the Neurosciences*, 24, 9–25.
- Li, X., Xu, D., Zhou, H., and Li, L. (2018), "Tucker tensor regression and neuroimaging analysis," *Statistics in Biosciences*, 10, 520–545.
- Marek, S. and Dosenbach, N. U. (2018), "The frontoparietal network: function, electrophysiology, and importance of individual precision mapping," *Dialogues in clinical neuroscience*, 20, 133.
- Mennes, M., Kelly, C., Colcombe, S., Castellanos, F. X., and Milham, M. P. (2013), "The extrinsic and intrinsic functional architectures of the human brain are not equivalent," *Cerebral cortex*, 23, 223–229.
- Morita, T., Asada, M., and Naito, E. (2016), "Contribution of neuroimaging studies to understanding development of human cognitive brain functions," Frontiers in human neuroscience, 10, 464.
- Neal, R. M. and Hinton, G. E. (1998), "A view of the EM algorithm that justifies incremental, sparse, and other variants," in *Learning in graphical models*, Springer, pp. 355–368.
- Nebel, M. B., Lidstone, D. E., Wang, L., Benkeser, D., Mostofsky, S. H., and Risk, B. B. (2022), "Accounting for motion in resting-state fMRI: What part of the spectrum are we characterizing in autism spectrum disorder?" *NeuroImage*, 257, 119296.
- Niendam, T. A., Laird, A. R., Ray, K. L., Dean, Y. M., Glahn, D. C., and Carter, C. S. (2012), "Meta-analytic evidence for a superordinate cognitive control network subserving diverse executive functions," *Cognitive, Affective, & Behavioral Neuroscience*, 12, 241–268.
- Rapuano, K. M., Rosenberg, M. D., Maza, M. T., Dennis, N. J., Dorji, M., Greene, A. S., Horien, C., Scheinost, D., Constable, R. T., and Casey, B. (2020), "Behavioral and brain signatures of substance use vulnerability in childhood," *Developmental cognitive neuroscience*, 46, 100878.
- Satterthwaite, T. D., Elliott, M. A., Gerraty, R. T., Ruparel, K., Loughead, J., Calkins, M. E., Eickhoff, S. B., Hakonarson, H., Gur, R. C., Gur, R. E., et al. (2013), "An improved framework for confound regression and filtering for control of motion artifact in the preprocessing of resting-state functional connectivity data," *Neuroimage*, 64, 240–256.
- Sethuraman, J. (1994), "A constructive definition of Dirichlet priors," *Statistica sinica*, 639–650.

- Shen, J. and He, X. (2015), "Inference for subgroup analysis with a structured logistic-normal mixture model," *Journal of the American Statistical Association*, 110, 303–312.
- Shen, X., Finn, E. S., Scheinost, D., Rosenberg, M. D., Chun, M. M., Papademetris, X., and Constable, R. T. (2017), "Using connectome-based predictive modeling to predict individual behavior from brain connectivity," *nature protocols*, 12, 506–518.
- Shen, X., Tokoglu, F., Papademetris, X., and Constable, R. T. (2013), "Groupwise whole-brain parcellation from resting-state fMRI data for network node identification," *Neuroimage*, 82, 403–415.
- Stark, G. F., Avery, E. W., Rosenberg, M. D., Greene, A. S., Gao, S., Scheinost, D., Todd Constable, R., Chun, M. M., and Yoo, K. (2021), "Using functional connectivity models to characterize relationships between working and episodic memory," *Brain and Behavior*, 11, e02105.
- Tibshirani, R. (1996), "Regression shrinkage and selection via the lasso," *Journal of the Royal Statistical Society: Series B (Methodological)*, 58, 267–288.
- Tzikas, D. G., Likas, A. C., and Galatsanos, N. P. (2008), "The variational approximation for Bayesian inference," *IEEE Signal Processing Magazine*, 25, 131–146.
- Van Den Heuvel, M. P., Stam, C. J., Kahn, R. S., and Pol, H. E. H. (2009), "Efficiency of functional brain networks and intellectual performance," *Journal of Neuroscience*, 29, 7619–7624.
- Vriend, C., Wagenmakers, M. J., Van den Heuvel, O. A., and Van der Werf, Y. D. (2020), "Resting-state network topology and planning ability in healthy adults," *Brain Structure and Function*, 225, 365–374.
- Wig, G. S. (2017), "Segregated systems of human brain networks," *Trends in cognitive sciences*, 21, 981–996.
- Xu, D. (2020), "Sparse Symmetric Tensor Regression for Functional Connectivity Analysis," arXiv preprint arXiv:2010.14700.
- Yeo, B. T., Krienen, F. M., Sepulcre, J., Sabuncu, M. R., Lashkari, D., Hollinshead, M., Roffman, J. L., Smoller, J. W., Zöllei, L., Polimeni, J. R., et al. (2011), "The organization of the human cerebral cortex estimated by intrinsic functional connectivity," *Journal of neurophysiology*.
- You, C., Ormerod, J. T., and Mueller, S. (2014), "On variational Bayes estimation and variational information criteria for linear regression models," *Australian & New Zealand Journal of Statistics*, 56, 73–87.

- Zhang, H. and Singer, B. H. (2010), Recursive partitioning and applications, Springer Science & Business Media.
- Zhou, H., Li, L., and Zhu, H. (2013), "Tensor regression with applications in neuroimaging data analysis," *Journal of the American Statistical Association*, 108, 540–552.